Journal of Marine Research, 64, 173–194, 2006

Journal of
MARINE RESEARCH

Volume 64, Number 2

An estuarine box model of freshwater delivery to the coastal ocean for use in climate models

by Richard W. Garvine[1] and Michael M. Whitney[2]

ABSTRACT

Present day climate models employ a coarse horizontal grid that is unable to fully resolve estuaries or continental shelves. The importation of fresh water from rivers is critical to the state of deep ocean stratification, but currently the processing of that fresh water as it passes from the river through the estuary and adjacent shelf is not represented in the coastal boundary conditions of climate models. An efficient way to represent this input of fresh water to the deep ocean would be to treat the estuary and shelf domains as two coupled box models with river water input to the estuarine box and mixed fresh water and coastal water output from the shelf box to the deep ocean.

We develop and test the estuary box model here. The potential energy anomaly ϕ is found from the five competing rates of change induced by freshwater inflow, mixed water outflow to the shelf, tidal mixing, surface heat flux, and wind-induced mixing. When application of the box model is made to the Delaware estuary, the wind mixing term contributes little. A 15-year time series of ϕ compares surprisingly well with the calculations of a three-dimensional numerical model applied to the Delaware estuary. The results encourage the future development of a shelf box model as the next step in constructing needed boundary conditions for input of fresh water to the deep ocean component of coupled climate models.

1. Introduction

River discharge of fresh water plays a much larger role in climate dynamics than would be guessed on the basis of its total volume flux. The global discharge of all gauged river sources is about 1.2×10^6 m^3 s^{-1} or 1.2 Sv (John Milliman, pers. comm.). This flux is

1. The Graduate School of Marine Studies, University of Delaware, Newark, Delaware, 19716, U.S.A. ***email: rgarvine@udel.edu***

2. Department of Marine Sciences, University of Connecticut, Groton, Connecticut, 06340, U.S.A.

dwarfed by the deep ocean gyres, such as the North Atlantic subtropical gyre, with a horizontal plane transport of about 120 Sv, or the North Atlantic meridional overturning cell with a vertical plane transport of about 20 Sv. The greatest influence of riverine fresh water, instead, is in its action as a catalyst for promoting ocean stratification, as measured by the available potential energy (APE) it brings, especially at high latitudes where the surface density is largely determined by the salinity with little effect by the temperature.

The sensitivity of the oceanic thermohaline circulation to changes in freshwater discharge is most pronounced in the meridional overturning of the North Atlantic and the subsequent production of North Atlantic Deep Water (NADW). Using a simplified, coupled ocean and atmosphere model, Rahmstorf (1995) showed that increase in total freshwater flux to the ocean as small as 0.06 Sv (five percent of the present total) could substantially reduce or even shut down the overturning with potentially severe impact on the climate of the North Atlantic and western Europe. Fairbanks (1989) estimated that the glacial melt associated with a continental ice sheet would generate 0.44 Sv of freshwater input for several thousand years. Dickson *et al.* (2002) found strong evidence from hydrographic records that significant freshening of the North Atlantic has been in progress for the past 40 years. Accurate prescription of freshwater flux from rivers can be expected to play a major role in climate modeling.

Wunsch (2005), on the other hand, suggested that the changes that produced such sharp shifts in climate as the Younger-Dryas event ca. 12,000 B.P. could have been caused by rapid shifts in the distribution of tidal mixing. A significant part of the tide is dissipated on the continental shelves of the world ocean in the present time, but during the height of glaciation, little shelf tidal dissipation would have been possible because most shelves were dry land. The flooding and drying of the continental shelf could contribute to hysteresis in the climate response to forcing.

River discharge of fresh water may operate in a similar manner as shelves flood and dry. In the present flooded condition, freshwater plumes turn anticyclonically at their estuary's mouth and become coastally trapped, while flowing downshelf, at right angles to an across-shelf pathway for maximum delivery to the deep ocean. A notable exception occurs with the Columbia River which flows directly into the deep ocean.

This deferred entry into the deep ocean may occur on a much larger scale than a single plume and coastal current. Chapman and Beardsley (1989) argued that the mean freshwater flow to the south in the Middle Atlantic Bight originated far upshelf as a continuous buoyancy-driven coastal current. Beginning with the West Greenland Current, this water flows past Baffin Island to the Labrador shelf and ultimately to the Scotian shelf, the Middle Atlantic Bight shelf, and finally, after a journey of 5000 km from the Arctic, into the deep ocean at Cape Hatteras. Khatiwala *et al.* (1999) refined these ideas with more extensive oxygen isotope data and showed that the greater part of this long coastal current originated in the Baffin Island Current with the St. Lawrence River adding another third to the total that reached the Scotian Shelf. Such coastal trapping of fresh water on shelves when they are flooded during interglacial times allows extended opportunity for mixing with shelf water, especially as upwelling events transpire (Fong and Geyer, 2001 and Sanders and Garvine, 2001). In contrast, with a dry shelf during glacial times, fresh water would be directly injected into the deep ocean by the rivers at the shelfbreak, much as the Columbia River outflow does now. The amount of fresh water with its high potential energy delivered to the deep ocean should have been much greater then than at present.

Coupled climate models, such as RM15 and RM30 (Dixon *et al.,* 2003), have recently been developed at the National Oceanic and Atmospheric Administration's Geophysical Fluid Dynamics Laboratory (GFDL). They are used by scientists and policy-makers to understand projected climate change over centennial time scales. These models are typical of the current generation of climate models which contain land, ocean, sea-ice, and atmospheric submodels. The hydrological cycle is highly sophisticated. Fresh water evaporated from the surface of the ocean model falls as rain from the atmospheric model onto the land model, which then returns the fresh water via rivers to the ocean model. Miller *et al.* (1994) recognized the importance of accurate flux of fresh water on a global basis. They developed a model for the freshwater discharge and the orientation of the channel near the mouth which they applied to the 43 largest rivers (by discharge) world wide.

Because climate models are stressed for computational time, large horizontal grid sizes are dictated, usually a degree of latitude. Continental shelves and estuaries have scales of the order of 100 km, or less. Shelves and estuaries, then, currently cannot be resolved by these models. Instead their effects need to be included parametrically or as a submodel. Following this logic, freshwater input has been modeled by simply importing river water at *zero* salinity directly into the model grid within the surface layers of the deep ocean (Miller and Russell, 1997; Dixon, private communication), resulting in stratification much higher than climatology (Levitus *et al.*,1995).

Lee *et al*. (2005) show that prior to freshwater injection in the deep ocean model, inclusion of tidal mixing of river water with shelf water in coastal areas reduces the sea surface temperature and salinity errors of the direct injection method. The delivery of fresh water from rivers and melting ice across the shelf into the deep ocean is likely to be controlled by nontidal as well as tidal shelf processes, none of which is well understood. The need therefore exists for soundly based parameterizations of across-shelf transport of fresh water over the entire route between rivers and the deep ocean.

In their present state of development coupled climate models could benefit from more realistic boundary conditions for freshwater input along their 'coastal' boundaries. One practical method to achieve this would be to represent the estuary and shelf from which terrestrial fresh water comes as two adjoint box models, each operating in bulk fashion, one representing the estuary and the other the shelf. Figure 1 shows the idea schematically. The primary input to the first box would be fresh water delivered to the estuary from a river. This need has been anticipated by Miller and Russell (1997) and Miller *et al.* (1994). In a global climate model their results could be used handily as inputs to the estuary box.

Processes in the estuarine box would include the impact of tidal mixing in the estuary

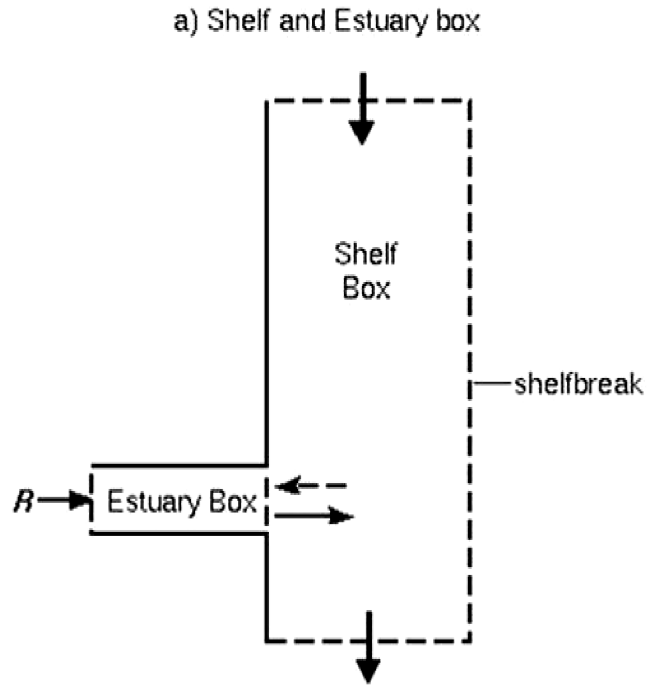

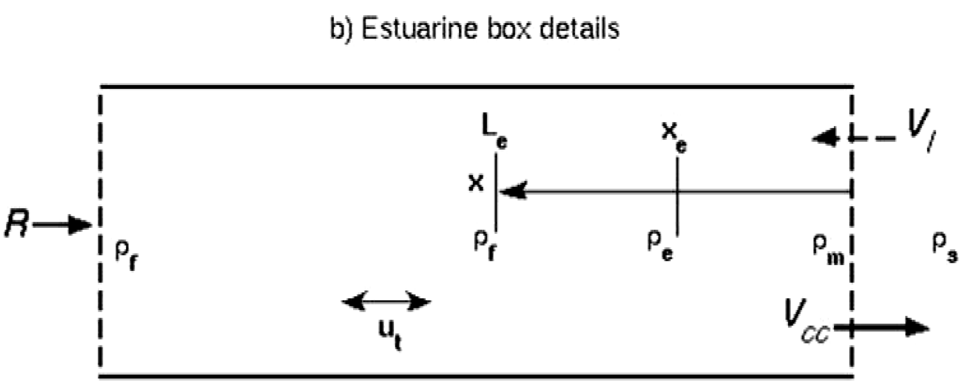

Figure 1. (a) A schematic showing the essential configuration of the estuary and shelf box models. The dashed lines symbolize open boundaries for the shelf box; arrows denote fluxes with the dashed arrow indicating lower layer shelf flow into the estuary. R indicates river inflow to the estuary. (b) A visual display of properties used in the text and their symbols. Note the four distinct densities: ρ_r,ρ_s,ρ_e,ρ_m representing the river, shelf, estuary mean, and estuary mouth, respectively. V_{cc} indicates the volume flux of the upper layer from the estuary into the coastal current, V_l the lower layer landward volume flux, R the river discharge, and u_t the tidal current amplitude. x is distance landward from the mouth, L_e is the length of the salt intrusion where fresh water is reached, and x_e the distance corresponding to half the estuarine surface area.

and the export of mixed river and shelf water to the shelf. The shelf box would take up there, reckoning in the effects of shelf tidal mixing and particularly of the straining and mixing produced by coastal upwelling circulation (Fong and Geyer, 2001; Sanders and Garvine, 2001).

In Section 2 we develop the estuarine model component or box. (The shelf box is planned for a subsequent paper.) In Section 3 we simplify this model momentarily to gain insight into the physical processes, then in Section 4 apply the full box model to the Delaware estuary where there are adequate field observations. In Section 5 we compare box model results with these observations and with numerical model results. Section 6 concludes the paper.

2. Box model development

Box models have a long history of use in the ocean sciences. Stommel (1961) used a box model to study the ocean thermohaline circulation and found bifurcated solutions with important climate implications. There are many examples of box model applications to estuaries (Hamilton *et al.*, 1985; Viera, 1985; and Roson *et al.*, 1997). Recently, Austin (2002) developed one for application to the salt budget for Chesapeake Bay. Here we develop a similar model, and focus on the density or, equivalently, the potential energy budget. This is the first step in a program to link with a companion box model for the adjacent shelf that will ultimately deliver the potential energy associated with the terrestrial fresh water to the deep ocean. The essential features of the adjoint boxes for estuary and shelf are shown in Figure 1.

What variables should the box model provide for use as physical boundary conditions on the deep ocean? The volume flux, momentum flux, and energy flux all seem candidates. But as we showed in Section 1, the volume flux of fresh water issuing from even a large river is negligible on the deep ocean scale. The kinetic energy content is also slight for freshwater delivery to the deep ocean, as a simple scaling argument shows.

The kinetic energy density is $\rho_0 q^2/2$ where q is the flow speed. The available potential energy/unit volume is given by Cushman-Roisin (1994) as $\rho_0 N^2 h^2/2$ where ρ_o is the reference density, N the buoyancy frequency, and h the vertical displacement of an isopycnal. For a buoyant coastal plume, h is approximately the plume depth. Hence, the ratio of kinetic to potential energy is $(q/Nh)^2 \equiv Fr^2$, the internal Froude number squared, typically quite small compared to unity. Consequently we expect the bulk of the energy content associated with buoyant river discharge to be in the form of potential energy. Other variables may be of interest, but the most essential is the potential energy.

The combination of potential energy as the primary dependent variable with two coupled boxes is analogous to analysis of the voltage in two parallel electrical circuits. Instead of solving Maxwell's equations for the three-dimensional, time dependent electric and magnetic field vectors, we employ the empirical formulation of lumped circuit theory with its bulk properties, such as resistance, capacitance, and inductance.

The particular variable we focus upon is the potential energy anomaly introduced by

Simpson and Hunter (1974) for analysis of shelf sea fronts and since used by Simpson and co-workers for a wide variety of insightful works on the stratification of estuaries and shelf regions. One could use the vertically averaged buoyancy or density for the primary dependent variable, but use of the potential energy anomaly in an estuarine or shelf setting allows us to better estimate the empirical constants that arise in the budget from those found by Simpson and co-workers.

We define the potential energy anomaly as

$$\phi \equiv \frac{g}{h}\int_{-h}^{0} (\rho - \rho_0) z dz$$

where ρ_0 is the reference state density.

This is set at the mean density of adjacent shelf water for the estuarine box; for the shelf model it would be the mean density of slope water beyond the shelfbreak.

By its definition ϕ is depth independent but varies horizontally and with time. The relationship of ϕ to the potential energy density is close. For example, for a buoyant outflow of stratification N and depth h, $\phi = \rho_0 (Nh)^2/6$. The vertically averaged potential energy/ unit volume for this feature is $\rho_0 (Nh)^2/2 = 3\phi$. The units of ϕ are Jm^{-3}. For a layer of depth h and uniform density ρ_1, $\phi = (\rho_0 - \rho_1)gh/2$. For further details, see the Appendix or the many papers by Simpson and co-workers treating the development of prescriptive models of stratified flows in estuaries and on continental shelves.

An important property of the potential energy budget is the flux across a vertical plane or section. Consider an area dA on the section. The differential flux of potential energy carried into the box in time dt per unit area is

$$dP = g(\rho - \rho_0) z u dt$$

where udt is the inflowing differential volume per unit area of the section in time dt. The vertically averaged rate of change of potential energy over the whole section is then

$$\Omega = \frac{1}{h}\iint_A \frac{dP}{dt} dA = \frac{1}{h}\iint_A g(\rho - \rho_0) z u dA.$$

We will neglect across channel variations over the breadth, giving

$$\Omega = \frac{gA}{h^2}\int_{-h}^{0} (\rho - \rho_0) z u dz. \tag{1}$$

The analogous expression for surface heat flux is (Simpson *et al.*, 1990) $\Omega = \alpha g \dot{Q} A_e/(2C_p)$ where α is the thermal expansion coefficient, $\dot{Q}$ is the vertical heat flux, A_e the surface area of the estuary, and C_p the specific heat of sea water. Unlike this result, the horizontal flux represented in (1) requires an assumption about how u and ρ are distributed in the vertical. To apply (1) to the inflowing fresh water we assume that $\rho = \rho_r$ = constant, the river water density (see Fig. 1b for a schematic with labels for the estuarine variables), while, approximating the flow state as one of hydraulic balance: $u = u_s[1 - \omega(z/h)^2]$. This gives zero vertical shear at the free surface where the current is u_s. The near bottom current is $(1 - \omega)u_s$ with $0 < \omega < 1$, the limits giving uniform current and no slip at the bottom, respectively. Using the profile for u and inserting in (1) gives

$$\Omega_1 = \left(1 - \frac{\omega}{2}\right) gA(\rho_0 - \rho_r)\,\frac{u_s}{2}.$$

The volume flux is closely related to the potential energy flux.

$$V = \iint_A u\,dA = \left(1 - \frac{\omega}{3}\right) Au_s = R.$$

Here we equate the volume flux to R, the river discharge. Substitution for Au_s in the expression for Ω_1 gives

$$\Omega_1 = P(\rho_0 - \rho_r)gR/2$$

where

$$P = \left(1 - \frac{\omega}{2}\right) \Big/ \left(1 - \frac{\omega}{3}\right).$$

The profile constant P has a narrow range from 1 at $\omega = 0$ to 0.75 at $\omega = 1$, so there is little impact of profile shape on the freshwater flux contribution.

The flux at the mouth is found similarly, but unlike the fresh water contribution it is clearer here if we distinguish the mean lower layer landward-flowing water from the mean seaward flow. As we explain below, the landward flow contributes nothing to the potential energy flux. For the seaward flow we adopt a linear density variation with depth (N = constant) and surface value of ρ_m.

$$\rho - \rho_0 = (\rho_m - \rho_0) - \frac{\rho_0}{g} N^2 z.$$

The second term gives the variation with depth. Its magnitude for the estuary of application in this paper (the Delaware estuary) is small compared to the first term, so we will neglect it. We choose a linear velocity profile in keeping with thermal wind balance and a vertically uniform across-stream density gradient. We impose no-slip at the bottom for simplicity. Thus, $u = u_t(1 + z/h)$. This gives

$$V = A_m u_t/2 = V_{cc} \quad \text{and} \quad \Omega_2 = -gV_{cc}(\rho_0 - \rho_m)/3.$$

Here we equate the volume flux V to the buoyancy-driven coastal current volume flux V_{cc} that continues on the shelf beyond the estuary.

As shown in the Appendix, one may relate the total volume flux V across a vertical section to that of fresh water, Q:

$$Q = \iint_A \frac{(\rho_0 - \rho)}{(\rho_0 - \rho_r)} q_n dA = \frac{(\rho_0 - \rho)}{(\rho_0 - \rho_r)} \iint_A q_n dA = \frac{(\rho_0 - \rho)}{(\rho_0 - \rho_r)} V.$$

Accounting for Q will enable the box model to conserve fresh water, even as it emerges from the river and undergoes mixing with estuary and shelf water. Fresh water will then act as a tracer in the deep ocean that is important to climate modelers.

The task is to assess the time rate of change of ϕ from fluxes across the boundaries, both vertical and horizontal, and from interior processes. An initial state is imposed from which the model is brought forward in time by summing all the rates of change that are active, sources, sinks, inflows, and outflows. While we could seek to resolve tidal frequency variations, such as Simpson *et al.* (1990) did, here, we limit the model to subtidal frequencies, as the intended analysis is for climate models.

We compute the total potential energy in the estuary from

$$\Phi \equiv \iint_A \phi dxdy \equiv A_e \phi_e$$

where Φ (units of Jm^{-1}) is the sum of the potential energy in the estuary, A_e is the surface area of the estuary, and ϕ_e is the area averaged potential energy anomaly (Jm^{-3}).

The equation expressing the budget of ϕ_e is (Simpson *et al.,* 1990 and 1991):

$$\frac{d\Phi}{dt} = \sum_{i=1}^{N} \Omega_i, \quad \phi_e = \Phi/A_e. \tag{2}$$

Here Ω_i are the rates associated with N distinct processes. For the present application, $N = 5$.

The solution for ϕ_e has limitations. It does not determine the density distribution with depth at future times, only the depth averaged potential energy per unit depth. An indefinite number of density profiles can be constructed for the same value of ϕ_e. The simplest is the depth uniform density for which $\phi_e = (\rho_s - \rho_e)gh/2$. Other examples are given in the Appendix.

As an example of application to climate models, one would obtain the shelf box model time series of ϕ and volume flux Q at a box outflow element and constrain the climate model's corresponding boundary element so that its ϕ and Q match the vertically integrated potential energy anomaly and volume flux. For example, if the climate model had constant N density structure with surface density ρ_{surf}, then at a boundary node of the

Table 1. Potential energy anomaly rate components.

Rate symbol	Name	Expression
Ω_1	Freshwater influx from river	$Pg(\rho_s - \rho_r)R/2$
Ω_2	Outflux to coastal current	$-g(\rho_s - \rho_m)V_{cc}/3$
Ω_3	Tidal mixing	$-\dfrac{4\varepsilon}{3\pi} C_d \rho_s u_t^3 A_e/h$
Ω_4	Solar radiation	$\dfrac{\alpha g Q_s A_e}{2C_p}$
Ω_5	Wind mixing	$-\delta \kappa_s \rho_a W_x^3 A_e/h$

climate model, the values of N and ρ_{surf} would not be independent but instead would be constrained by $(\rho_0 - \rho_{surf})gh/2 + \rho_0(Nh)^2/6 = \phi_i$. At the same boundary node the normal velocity v_i is set by V_i/A_i where A_i is the vertical sectional area of the climate model's coastal boundary. Q_i would be computed using Eq. (A3) (see the Appendix). The expressions for these rates appear in Table 1 (see Fig. 1b for a schematic view of the estuary box and its variables). The river flux of fresh water generates Ω_1. Here R is the river discharge of fresh water at density ρ_r. Shelf water (the reference density ρ_0 in this model) has density ρ_s. The factor P is set by the profiles of current and density at the river inflow. The expression for Ω_2, the flux of mixed water to the shelf, is similar, but carries a minus sign because the volume flux V_{cc} in the seaward flowing layer is directed out of the box and has density ρ_m at the mouth.

In principle, another contribution to the budget would be made from V_l, the deeper, landward flowing companion to V_{cc}, but it has shelf water density, here the reference density, and so makes no contribution to the estuarine potential energy budget. In a shelf box model it would require such accounting. Imposing bulk mass continuity on the box for the subtidal frequency flow and a weakly nonlinear tidal regime gives $V_l = V_{cc} + R - St$ where St is the mean Stokes volume transport at the mouth (Longuet-Higgins, 1969).

We compute V_{cc} empirically using a linear regression with subtidal wind and river discharge as independent variables of the form

$$V_{cc} = \bar{V}_{cc} + a_1(W_x - \overline{W_x}) + a_2(R - \bar{R}).$$

Here overbars denote long-term means, W_x is the wind component along the estuary axis, positive seaward, R is the river discharge at 5 day's lag from the river discharge gauge, and a_1 and a_2 are site dependent constants obtained from mooring data presented by Sanders and Garvine (2001).

Note the factor $(\rho_s - \rho_m)$ in the expression for Ω_2. This is critical to coupling the response of the system to the forcing, as ρ_m is related to ρ_e. We adopt a linear variation of density with x to connect these two densities:

$$\rho_e - \rho_r = \frac{L_e - x_e}{L_e}(\rho_m - \rho_r). \tag{3}$$

Here L_e is the landward distance from the mouth where the salinity reaches fresh water value and x_e is the axial location where the density takes on the estuary area averaged value ρ_e. This axial location is set where half the surface area of the estuary is seaward and half landward. We chose a linear distribution of density or salinity as the simplest possible. Furthermore, for the Delaware estuary application, a linear variation closely describes the observed axial variation (Garvine *et al.*, 1992). The expression in (2) is complete upon replacing ρ_e with $\rho_s - 2\phi_e/gh$. (See Eq. (2) in the Appendix.)

Tidal mixing, Ω_3, is represented by the cube of the root mean square current amplitude in the estuary. The constants ε and C_d represent the mixing efficiency of the tide and the bottom drag coefficient, respectively (Simpson *et al.,* 1991). We used a mean value for u_t, the root mean square tidal current amplitude, and a modulation about the mean with a 14-day harmonic variation to represent the impact of neap and spring tides on mixing. A_e and h represent the estuarine surface area and mean water depth, respectively, so that their product gives the estuarine volume.

The estuarine gravitational circulation itself can contribute to the stratification through the coupled low frequency current and density gradient. Simpson *et al.* (1991) give a form for estimating it. This mechanism was weak for the present application, though it might be competitive in an estuary with greater stratification. This term is not included in the present results.

In Ω_4, the radiation heat flux, the thermal coefficient of expansion is $\alpha = 1.7 \times 10^{-4}$/K, C_p is the specific heat of sea water (4200 J/(kg-K)), and Q_s is the net solar radiation. For the latitude of 40N, Gill (1982, Chapter 1) shows a mean shortwave flux of 225 W/m^2 and a seasonal amplitude of 90 W/m^2. We adjusted the maximum to the time of the summer solstice. The contributions of sensible and latent heat were ignored. Wind mixing inside the estuary is modeled in Ω_5. This action results mainly from breaking surface waves. The constants δ and κ_s represent the mixing efficiency of the wind and the effective surface drag coefficient, respectively; ρ_a is the air density at sea level.

3. Analytical model

In this section we seek to gain preliminary insight into the box model's response to forcing by holding the variable parameters in the Ω_i of Table 1 fixed in time, including R, V_{cc}, u_t, Q_s, and W_x. Then (2) takes the form

$$\frac{d\phi_e}{dt} = J - K\phi_e. \tag{4}$$

Here J and K are constants given by:

$$J = \frac{Pg}{2A_e}(\rho_s - \rho_r)R + \frac{g}{3A_e}(\rho_s - \rho_m)V_{cc}\frac{x_e}{L_e - x_e} - \frac{4\varepsilon}{3\pi}C_d\rho_s\frac{u_1^3}{h} + \frac{\alpha g Q_s}{2C_p} - \delta\kappa_s\rho_a W_x^3/h$$

$$K = \frac{V_{cc}}{A_e h}\frac{L_e}{L_e - x_e}.$$

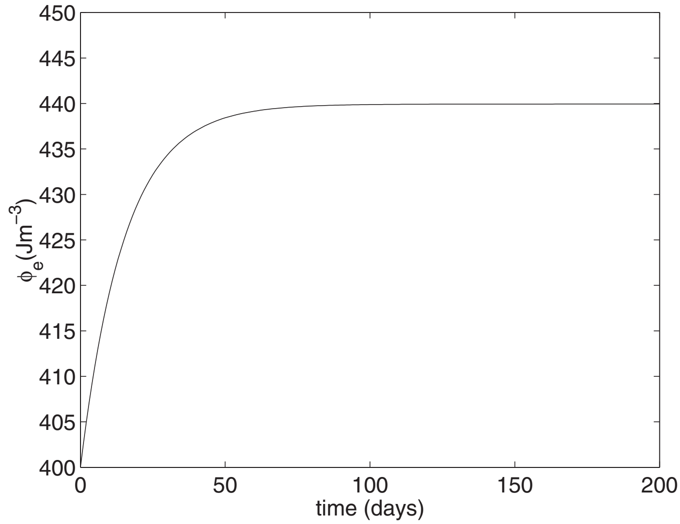

Figure 2. Analytical solution for the model response with major parameters (Table 1, right column) of the box model fixed.

These terms constitute a first order, linear ordinary differential equation. Austin (2002) found a similar linear equation for the salinity in his box model of the salt budget of Chesapeake Bay. The well known solution is:

$$\phi_e = \frac{J}{K} + \left(\phi_0 - \frac{J}{K}\right)e^{-Kt}.$$

Here ϕ_0 is ϕ_e at time zero. Note that from its definition $K > 0$, except for unusual events where the sign of V_{cc} reverses with subsequent landward flow. Consequently, we find two primary characteristics of ϕ_e in the box model: first, it varies on the time scale of K^{-1} and, second, it is convergent in time to the constant level *J/K*. K originates in the estuarine outflux to the coastal current. The coastal current term in (4), $-K\phi_e$, is the only term dependent on ϕ_e, providing essential feedback that results in a stable regime for the system. Note that we may approximate K by

$$K = \frac{V_{cc}L_e}{A_e h(L_e - x_e)} \approx \frac{V_{cc}}{A_e h}.$$

The approximate term on the right is the coastal current volume flux divided by the scale of the estuary volume. The time scale K^{-1} then is just the time for the coastal current to empty the estuary, once the freshwater inflow has been switched off. For the Delaware estuary, $V_{cc} \sim 9000\ \mathrm{m}^3\ \mathrm{s}^{-1}$, $A_e \sim 2 \times 10^9\ \mathrm{m}^2$, and $h \sim 8$ m, or the response time scale is about 2×10^6 s or about 23 days. Figure 2 illustrates the simple response. The initial value $\phi_0 = 400\ \mathrm{Jm}^{-3}$, a level typically found in the general results.

4. Application

Application to the Delaware estuary enabled us to compare the outcomes with an extensive field data set and with a standard numerical ocean model. This model was previously applied to simulate the circulation and mixing of Delaware estuary water with the adjacent inner continental shelf (Whitney and Garvine, 2005, 2006).

The Delaware estuary is a large coastal plain estuary of the well mixed or weakly stratified class. Tidal volume flux exceeds the flux of fresh water by a ratio of 230:1 and, as a result, the bulk vertical salinity or density change is only about 1 unit. The M_2 constituent is dominant. The climatological mean freshwater discharge is about 650 m^3/s of which it is reckoned that 58% enters the estuary at Trenton, NJ and the rest in the lower estuary. The estuary is shallow with a mean depth of 8 m. At the mouth the width is about 18 km. As the buoyant waters of the estuary depart the mouth, they are concentrated near the surface and on the right side of the estuary (viewed looking seaward). The light water there then makes an anticyclonic turn under Coriolis deflection and continues down the shelf as a buoyancy driven coastal current (Garvine, 1991; Münchow and Garvine, 1993a,b; Sanders and Garvine, 1996, 2001). Figure 3 shows the estuary and the inner shelf location of the three instrumented mooring lines where current, conductivity, and temperature data were collected for 4 months in 1993 during the season of high river discharge. The mooring data were suitable for calculating the flux of fresh water across the circular arc defined by the three moorings. (See Appendix.) This time series proved valuable for comparison of the box model results with observations.

Table 2 shows the values used for the different constants introduced in Table 1. Most of these are determined within 5-10% by the known physical properties of the system, such as the length L and area $A_{e.}$ The last four listed are dimensionless empirical constants found by Simpson *et al.* (1991) by comparison with observations.

Figure 4 shows the variations and levels of the rates Ω_i computed from the box model using observed data for river discharge and wind for 1993. The largest contributor, not surprisingly, is the river discharge followed closely (but with the opposite sign) by the coastal current efflux. Tidal mixing makes a persistent contribution to the reduction of the potential energy with modulation at the spring-neap period (14 days). (Only the mean tidal mixing term is plotted to maintain clarity, but the effect of the tidal modulation is readily seen in the curve marked "$d\Phi/dt$.") Solar heating makes a persistent and modest contribution in favor of potential energy. The impact of wind variations is visible in the high frequency fluctuations in the coastal current response. Wind mixing, however, was too small to be plotted.

A direct comparison of box model results with observations is shown in Figure 5. Here the estimated total flux of fresh water past the mooring array (Sanders and Garvine, 2001) is plotted for the duration of the mooring installation. The box model calculation for this flux is shown also. Generally it displays reduced variance and higher level than the observed. The time integrals of these freshwater fluxes for the period of the mooring installation were 1050 m^3/s for the observed vs. 1519 for the box model, giving a ratio of

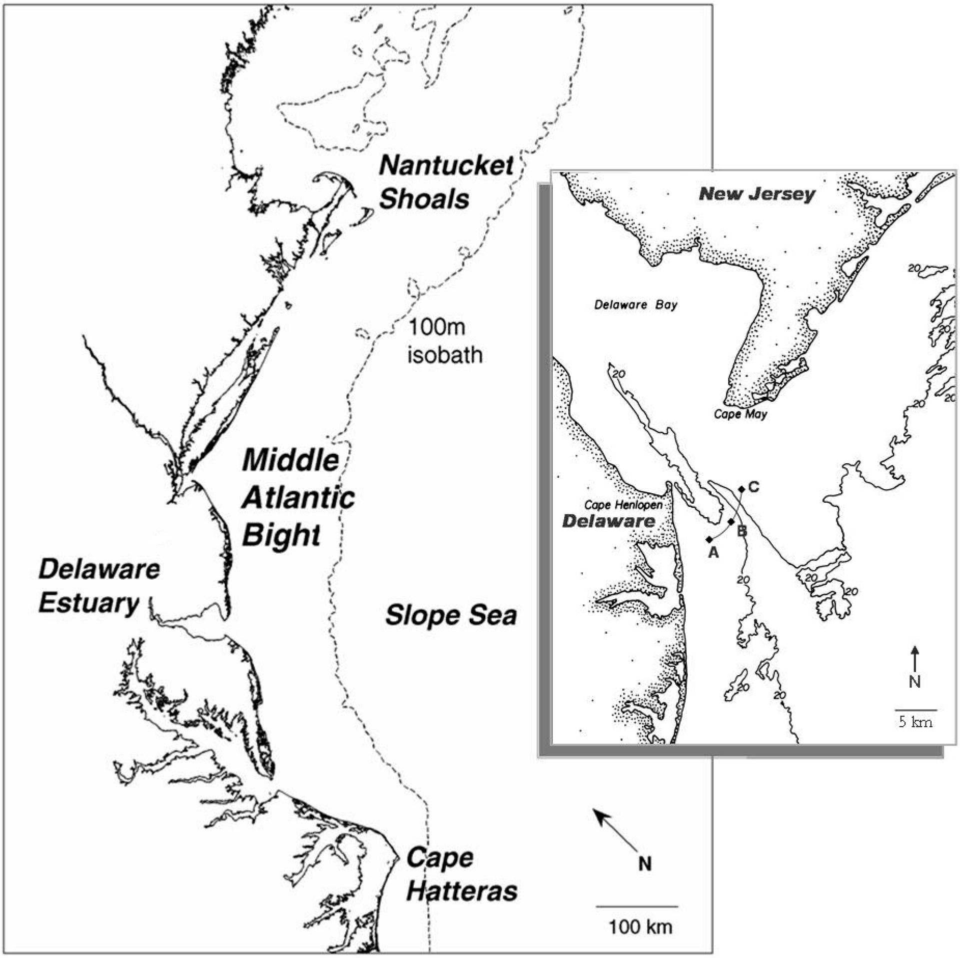

Figure 3. The large panel shows the shelf of the Middle Atlantic Bight which extends from Nantucket Shoals to Cape Hatteras. The figure has been rotated from North. The inset shows the Delaware estuary, the site of the application of the box model. North is upwards. Note the location of the mooring arc formed by moorings A,B, and C just beyond the estuary mouth. Volume flux of fresh water was computed from records at these sites and is shown in Figure 5. Isobaths in meters.

0.69. The correlation coefficient is 0.52. One explanation for the difference in levels of fresh water is that the mooring array effectively intercepted only a portion of the actual freshwater flux that was present, especially in times of high discharge when we would expect the plume breadth to expand.

5. Comparison with the numerical model

Whitney and Garvine (2005, 2006) applied the ocean model ECOM3d (Blumberg and Mellor, 1987) to the Delaware estuary and a large part of the adjacent continental shelf

Table 2. Values for model constants used in the Delaware application.

Symbol	Name	Value
ρ_s	Shelf water density	1024.6 kg/m^3
ρ_r	River water density	999.7 kg/m^3
L_e	Distance from estuary mouth to fresh water	97 km
x_e	Distance from estuary mouth to water of density ρ_e	30 km
A_e	Surface area of the Delaware estuary	2.1×10^9 m^2
u_t	Root mean square tidal current amplitude	0.6 m/s
u_{mod}	Tidal current amplitude modulation for neap-spring variations	0.12 m/s
$\bar{V}_{cc}$	Mean volume flux at mouth	8800 m^3/s
ω	Parameter of the current variations with depth	0.67
a_1	Regression coefficient between wind and volume flux	433 m^{-2}
a_2	Regression coefficient between river discharge and volume flux	2.54
ε	Tidal mixing efficiency	0.0038
δ	Wind mixing efficiency	0.039
κ_s	Drag coefficient for surface	6.4×10^{-5}
C_d	Drag coefficient for bottom	2.5×10^{-3}

with the main objective of simulating the Delaware Coastal Current and comparison of model and observations. This model was driven by wind stress, Delaware River discharge, and M_2 tidal currents. Surface heat flux was set at zero and shelf water had a uniform density. Using a wide variety of observational data on the Delaware Coastal Current and in the Delaware estuary, they found the model to provide a satisfactory simulation of the major features, such as the response to upwelling vs. downwelling wind stress and the variation of river discharge. Figure 6 displays the ϕ field in the estuary and shelf computed from their model results for 1993. The maximum value is 1492 (Jm^{-3}) which occurs at the entry of Delaware River water into the upper estuary, while the lowest is 0, corresponding to the reference density $\rho_s = 1024.6$ kg m^{-3}. Rapid depletion of ϕ is evident within the lower estuary as tidal mixing and the export of potential energy into the coastal current operate. The surviving energy is conveyed downshelf by the coastal current.

For comparison with the box model, we integrated ϕ over the entire estuary as a function of time and divided by the estuary surface area to give an averaged value for direct comparison with the box model. Both the models used identical river discharge and wind data. The numerical model was started a year prior to the box model to allow it to come to equilibrium with the tidal mixing processes. Then at the start of the box model the initial

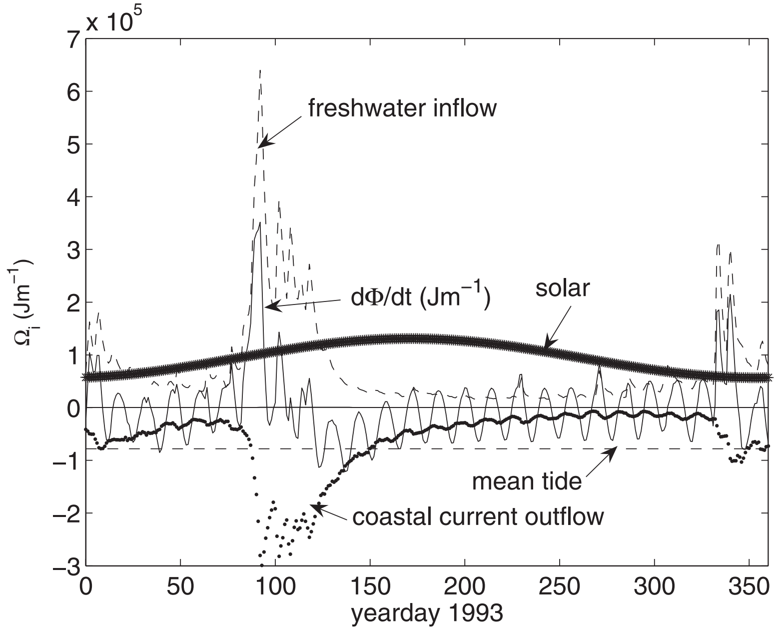

Figure 4. Time series of the rates of change of potential energy anomaly for four different competing mechanisms. The tidal term is shown only for the mean value because the spring-neap modulations would obscure other terms. The effect of these modulations appears in the curve labeled "$d\Phi/dt$."

value used was equated to that of the numerical model at that time. The models were run for a 15-year duration (5531 days) beginning in early 1989 and continuing to 2004. The agreement is surprisingly close (see Fig. 7) throughout the 15 years, especially at the lower frequencies. The correlation coefficient is 0.91. A linear regression of the form

$$\phi_{box} = a + b\phi_{3d}$$

yielded $a = 108$ (Jm^{-3}) and $b = 0.68$. The lower response of the box model compared to the numerical model is reflected in the value of $b = 0.68 < 1$. Correspondingly, the standard deviation of the box model is 34 vs. 45 for the numerical model. The standard deviation of the difference is 20. The greatest difference comes at the low values for the year, usually in summer when the river discharge is low and the solar radiation greatest. The numerical model had no solar input but used a zero heat flux surface boundary condition instead. Consequently, it would drop to lower values at times of low runoff compared to the box model. The mean values of ϕ were 349 and 354 Jm-3 for the box and numerical models, respectively. A least squares linear trend analysis of the box model time series showed a change of only 0.15 Jm-3 (0.042% of the mean) over the 15-year run. This indicates that the model reflects a plausible climatological balance for long time scales.

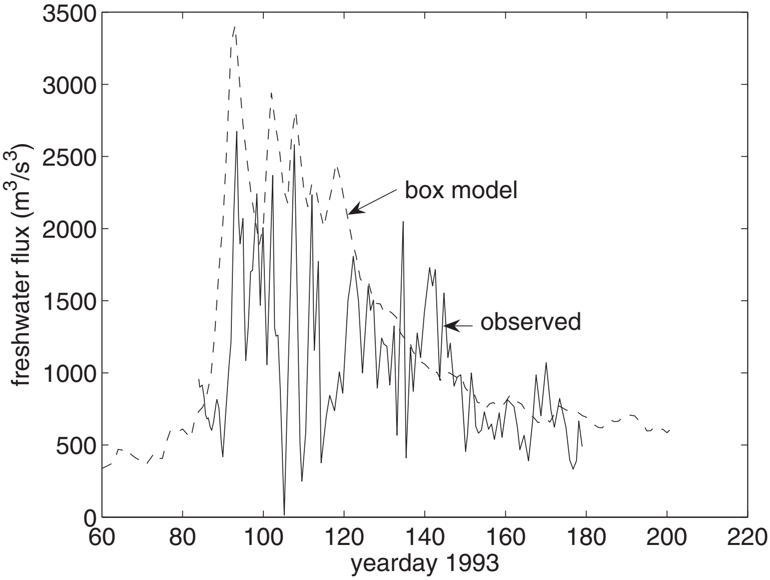

Figure 5. Time series of observed freshwater flux at the mooring arc (the solid curve, see Fig. 4) and from the box model.

6. Concluding remarks

We have developed a box model primarily intended for use in numerical models of climate dynamics where terrestrial freshwater delivery is critical. The model features the potential energy anomaly ϕ as the dependent variable and uses the formalism of Simpson *et al.* (1991), including its empirical constants, to fix a rate equation allowing simple time integration of ϕ forward from an initial state. The degree of the model's success is a direct consequence of the patience and skill of Simpson and his coworkers in their program of long-term model development.

What information is needed if this box model were to be applied to another estuary? Table 2 offers guidance. There are four types of inputs to the model: first, the empirical constants δ, κ, ε, and C_d obtained from Simpson *et al.* (1991); second, constant physical properties of the particular estuary and adjacent shelf: h, A_e, u_t , u_{tm}, ρ_a, $\rho_s - \rho_r$, ω, and ϕ_0 where u_{tm} is the modulation of the M_2 tidal current at the spring-neaps period; third, the time dependent driving functions R, W_x, and Q_s; fourth, the derived, time dependent property V_{cc}.

The model results are of interest beyond their demonstration of the submodel's utility. Some surprises result from application to the Delaware estuary. Only four major mechanisms compete in determining the average potential energy and the export rate of potential energy to the coastal ocean. These are the influx by fresh water from river inflow, the efflux into the coastal current, tidal mixing, and surface heat flux. Wind mixing could have been

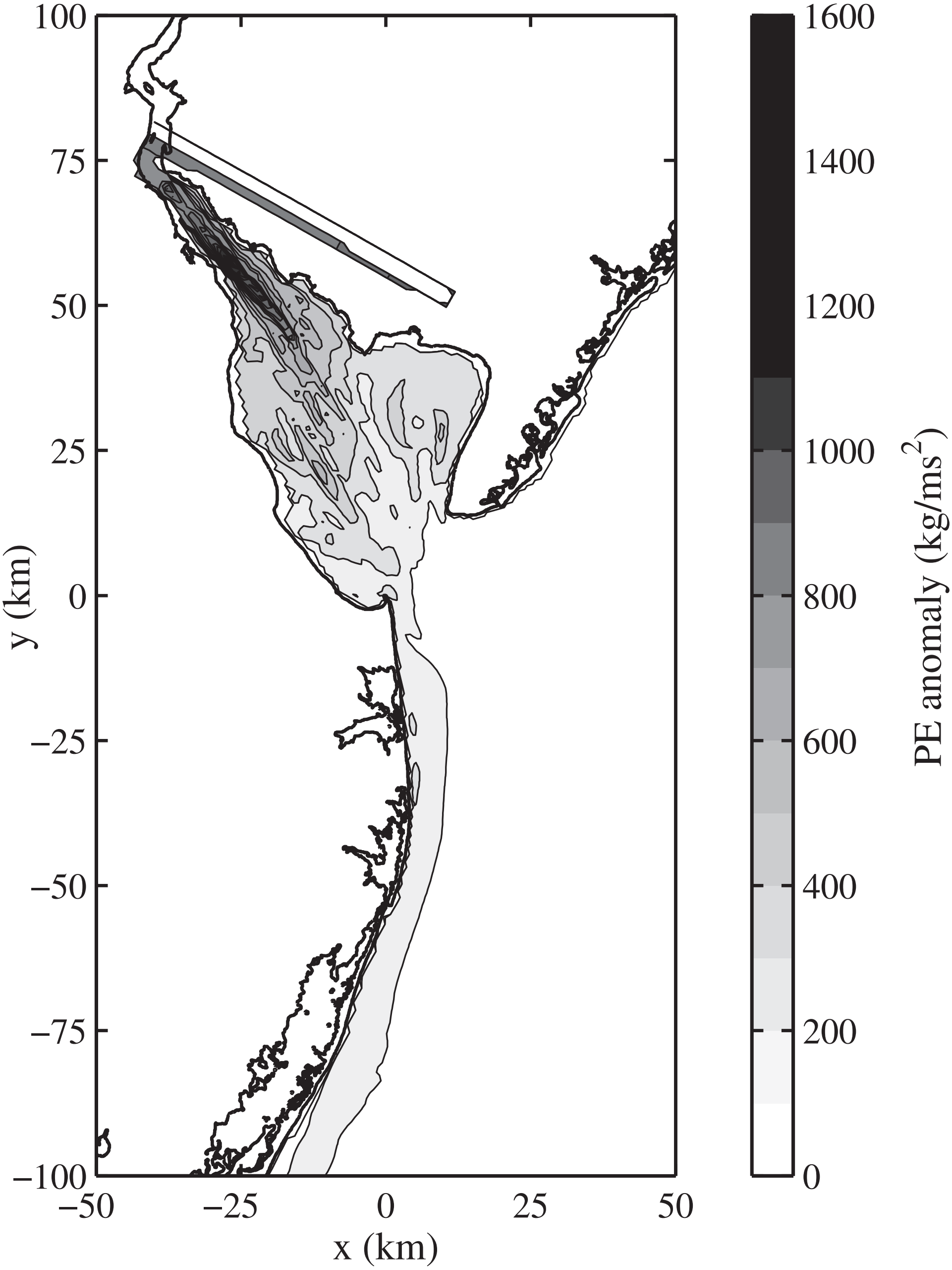

Figure 6. The field of ϕ_e from the numerical model for 14 April, 1993. The model configuration saves storage by folding the narrow upper estuary to keep it inside the model domain. Note the continuation of elevated potential energy in the coastal current flowing downshelf near the coast.

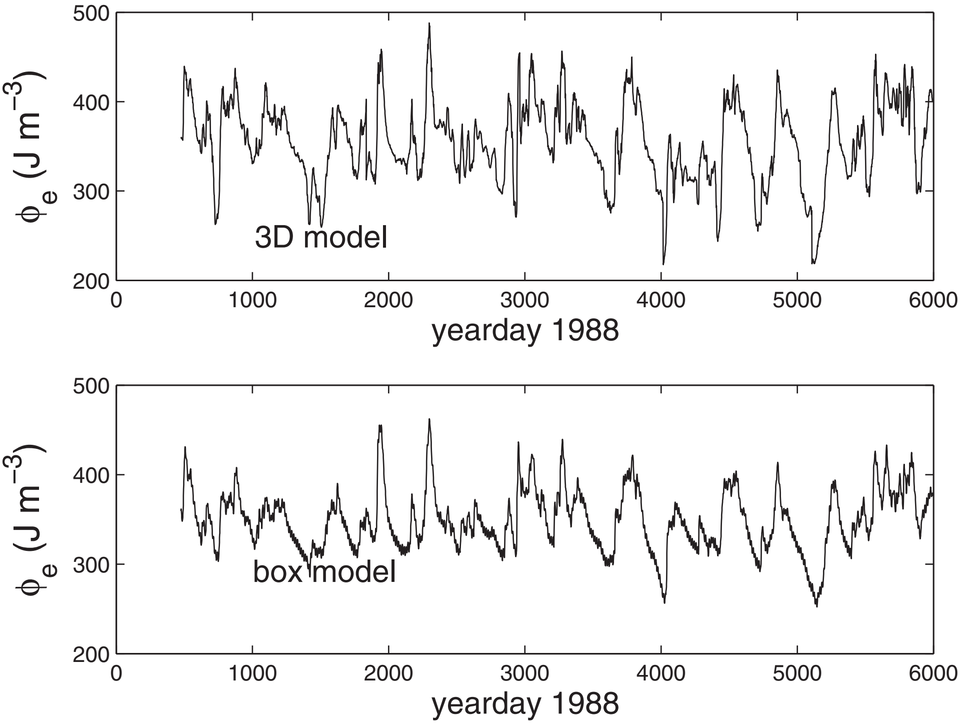

Figure 7. Time series for ϕ_e, the averaged estuary potential energy anomaly from the box model (lower panel) vs. the same for the three-dimensional model results (upper panel) for a period of 5531 days or 15 years.

ignored. The production of stratification by the estuarine circulation was found from the beginning to be small and was not further considered.

An analytic solution of a simplified version of the box model where the driving properties R, V_{cc}, u_t, Q_s, and W_x were held fixed in time showed that efflux to the coastal current forms a critical feedback mechanism. This allows adjustment to changes in the potential energy to reach a steady value after a time scale of the order necessary for the coastal current to empty the estuary.

The efflux of potential energy into the coastal current, when translated into the equivalent flux of fresh water, matched the temporal variation of the observed with a correlation of 0.52. The model time series compared surprisingly well with the results of a three-dimensional numerical model with a correlation of 0.91 and standard deviation of the difference of 20 Jm^{-3} compared to the mean value of 350 Jm^{-3}.

The estuarine box model is intended to produce a time series of the potential energy injected into coastal waters. In most settings where a substantial continental shelf is present, such as the shelf in the Middle Atlantic Bight of the east coast of the USA, a shelf box model joined with the present one will be necessary for prediction of the potential energy reaching the deep ocean. Added features not present in the estuary box would include the impact on the stratification by upwelling-favorable winds and loss of potential energy across the shelf break to slope water. For Arctic applications the melting and freezing of sea ice, including ice in rivers and estuaries, must also be accounted for.

For some other topographic settings, such as the west coast of much of North and South America, the depth increases so quickly beyond the mouth that the estuarine water is injected into deep water directly. This 'short circuit' is likely to be operable for the Columbia River off Oregon and Washington, for example. This behavior is likely to be similar to the state of injection during glaciation, as the rivers would have then run directly across the dry shelf, delivering nearly zero salinity water to the deep ocean beyond the shelfbreak.

Acknowledgments. We thank Brian Arbic for suggesting the study of river input of fresh water to the deep ocean for use in climate models. We also thank Alan Blumberg for access to the model ECOM3d. J. T. Reager competently ran the model to produce records continuously for the period 1984-2004. Ana Eguiluz, Glen Gawarkiewicz, Robert Hetland, Robert Houghton, Andreas Münchow, James O'Donnell, Felipé Pimenta, John Simpson, and Thomas Weingartner provided valuable comments on an earlier draft of the paper. Steven Lentz was especially helpful in finding an error in an earlier draft. Two anonymous reviewers made helpful suggestions. We were supported in this work by the National Science Foundation through grant OCE0220446 and by the National Oceanic and Atmospheric Administration (NOAA) through contract NA17EC2449.

APPENDIX

Properties of the potential energy anomaly ϕ

From its definition, ϕ is the potential energy anomaly of the local water column relative to the free surface and to the potential energy of a reference, such as a point in the adjacent deep ocean gyre. Following Simpson *et al.* (1991)

$$\phi \equiv \frac{g}{h}\int_{-h}^{0} (\rho - \rho_0) z dz. \tag{A1}$$

Note that our definition of the reference density differs from that of Simpson *et al.* (1991), as their reference is to the local mean density. As defined in (A1), $\phi \geq 0$ and has units of Jm^{-3}.

To fix ideas we derive the relation of ϕ to idealized vertical density structure. First, suppose we have a two-layer density profile with density ρ_1 and ρ_2 in the lower and upper layers, respectively. The interface is at $z = -d$. Use of (A1) then gives

$$\phi = \frac{g}{2h}[(\rho_0 - \rho_2)h^2 + (\rho_0 - \rho_1)d^2]. \tag{A2}$$

Two special cases are useful. (1) In the absence of a pycnocline $d \Rightarrow 0$, or

$$\phi = (\rho_0 - \rho_2)gh/2.$$

This case is relevant to the setting in the landward part of an estuary with weak stratification but with density different than ρ_0. The upper part of the Delaware estuary, for example, has a depth of about 8 m, a freshwater density $\rho_r = 999.7$ kg m^{-3}, and the adjacent shelf water a density of about 1024.6 kg m^{-3}, so that $\phi = 1082$ Jm^{-3}. (2) A strong pycnocline is present but the bottom layer density has reached the reference density, or

$$\phi = (\rho_0 - \rho_1)gh(d/h)^2/2.$$

The geometric factor $(d/h)^2$ will strongly affect the potential energy when d/h is small. If instead the density is continuously stratified over depth h with buoyancy frequency N and bottom density equal to the reference density,

$$\phi = \rho_0(Nh)^2/6.$$

Now we connect the flux of fresh water across the same section to the total volume flux. Here we again set shelf water density at the reference value ρ_0 and adapt the estuarine fractional freshwater anomaly as $F_{frac} = (S_0 - S)/S_0$ where S_0 is the shelf water mean salinity. The volume flux of fresh water passing through a vertical section of area A at normal velocity q_n is given by

$$Q = \iint_A F_{frac} q_n dA$$

where A is the total cross-sectional area of freshwater passage.

Employing an equation of state that assumes a linear relation between salinity and density

$$F_{frac} = \frac{S_0 - S}{S_0} = \frac{\rho_0 - \rho}{\rho_0 - \rho_r}$$

with ρ_r the density of the fresh water at the head of the estuary. ($S_r = 0$.)

Using these relations we find that for weak density variations over the section

$$Q = \iint_A \frac{(\rho_0 - \rho)}{(\rho_0 - \rho_r)} q_n dA = \frac{(\rho_0 - \rho)}{(\rho_0 - \rho_r)} \iint_A q_n dA = \frac{(\rho_0 - \rho)}{(\rho_0 - \rho_r)} V. \tag{A3}$$

REFERENCES

Austin, J. A. 2002. Estimating the mean ocean-bay exchange rate of the Chesapeake Bay. J. Geophys. Res., *107,* C11, 3192, doi 10.1029/2001JC001246.

Blumberg, A. F. and G. L. Mellor. 1987. A description of a three-dimensional coastal ocean circulation model, *in* Three-Dimensional Coastal Ocean Models, N. Heaps, ed., Amer. Geophys. Union, 1–16.

Chapman, D. C. and R. C. Beardsley. 1989. On the origin of shelf water in the Middle Atlantic Bight. J. Phys. Oceanogr., *19*, 389–381.

Cushman-Roisin, B. 1994. Introduction to Geophysical Fluid Dynamics, Prentice Hall, Engelwood Cliffs, NJ, 320 pp.

Dickson, R., I. Yashayaev, J. Meincke, W. Turrel, S. Pye and J. Holfort. 2002. Freshening of the deep North Atlantic Ocean over the past four decades. Nature, *416*, 832–837.

Dixon, K. W., T. L. Delworth, T. R. Knutson, M. J. Spelman and R. J. Stouffer. 2003. A comparison of climate change simulations produced by two GFDL coupled models. Global Planet. Change, *37*(1-2), 81–102.

Fairbanks, R. C. 1989. A 17,000 year glacio-eustatic sea level record: influence of glacial melting rates in the Younger-Dryas event and deep ocean circulation. Nature, *342*, 637–642.

Fong, D. A. and W. R. Geyer. 2001. The response of a river plume during an upwelling favorable wind event. J. Geophys. Res., *106*, 1067–1084.

Fratantoni, P. S. and R. S. Pickart. 2005. The western North Atlantic shelfbreak current system in summer. J. Phys. Oceanogr. (submitted).

Garvine, R. W. 1991. Subtidal frequency estuary-shelf interaction: Observations near Delaware Bay. J. Geophys. Res., *96*, 7049–7064.

Garvine, R. W., R. K. McCarthy and K.-C. Wong. 1992. The axial salinity distribution in the Delaware Estuary and its weak response to river discharge. Estuar. Coast. Shelf Sci., *35*, 157–165.

Gill, A. E. 1982. Atmosphere-Ocean Dynamics, Academic Press, International Geophysics Series, *30*, 662 pp.

Hamilton, P., J. T. Gunn and G. A. Cannon. 1985. A box model of Puget Sound. Estuar. Coast. Shelf Sci., *20*, 673–692.

Khatiwala, S. P., R. G. Fairbanks and R. W. Houghton. 1999. Freshwater sources to the coastal ocean off northeastern North America: Evidence from $H_2{}^{18}O/H_2{}^{16}O$. J. Geophys. Res., *106*, 18,241–18,255.

Lee, H.-C., A. Rosati and M. J. Spelman. 2005. Barotropic tidal mixing effects in a coupled climate model: Oceanic conditions in the Northern Atlantic. Ocean Model., (submitted).

Levitus, S., R. Burgett and T. P. Boyer. 1995. World ocean atlas 1994, 3, Salinity. NOAA/NESDIS E/OC21, US Dept. Commerce, Washington, DC.

Longuet-Higgins, M. S. 1969. On the transport of mass by time-varying ocean currents. Deep-Sea Res., *16*, 431–447.

Miller, J. R. and G. L. Russell. 1997. Investigating the interactions among river flow, salinity and sea ice using a global coupled atmosphere-ocean-ice model. Ann. Glaciol., *25*, 121–126.

Miller, J. R., G. L. Russell and G. Caliri. 1994. Continental-scale river flow in climate models. J. Climate, *7*, 914–928.

Münchow, A. and R. W. Garvine. 1993a. Buoyancy and wind forcing of a coastal current. J. Mar. Res., *51*, 293–322.

—— 1993b. Dynamical properties of a buoyancy driven coastal current. J. Geophys. Res., *98*, 20,063–20,077.

Rahmstorf, S. 1995. Bifurcations of the Atlantic thermohaline circulation in response to changes in the hydrological cycle. Nature, *378*, 145–149.

Roson, G., X. A. Alvarez-Salgado and F. F. Perez. 1997. A non-stationary box model to determine residual fluxes in a partially mixed estuary, based on both thermohaline properties: Application to the Ria de Arousa (NW Spain). Estuar. Coast. Shelf Sci., *44*, 249–262.

Sanders, T. M. and R. W. Garvine. 1996. Frontal observations of the Delaware Coastal Current. Cont. Shelf Res., *15*, 1009–1021.

—— 2001. Fresh water delivery to the continental shelf and subsequent mixing: An observational study. J. Geophy. Res., *27*, 087–27,101.

Simpson, J. H., J. Brown, J. Matthews and G. Allen. 1990. Tidal straining, density currents, and stirring in the control of estuarine stratification. Estuaries, *13,* 125–132.

Simpson, J. H. and J. R. Hunter. 1974. Fronts in the Irish Sea. Nature, *250*, 404–406.
Simpson, J. H., J. Sharples and T. P. Rippeth. 1991. A prescriptive model of stratification induced by freshwater runoff. Estuar. Coast. Shelf Sci., *33*, 23–35.
Stommel, H. 1961. Thermohaline convection with two stable end regimes. Tellus, *13*, 224–230.
Viera, M. E. C. 1985. Estimates of subtidal volume flux in mid-Chesapeake Bay. Estuar. Coast. Shelf Sci., *21*, 411–427.
Whitney, M. M. and R. W. Garvine. 2006. Simulating the Delaware Bay coastal buoyant outflow: Comparison with observation. J. Phys. Oceanogr., *36*, 3–21.
—— 2005. Wind influence on a coastal buoyant outflow. J. Geophys. Res., *110*, C3, C0315.
Wunsch, C. 2005. Speculations on a schematic theory of the Younger Dryas. J. Mar. Res., *63*, 315–333.

Received: *1 August, 2005*; revised: *1 November, 2005*.